THE CONSTANT INNER-DISK RADIUS OF LMC X-3: A BASIS FOR MEASURING BLACK HOLE SPIN

The Astrophysical Journal Letters, 718:L117–L121, 2010 August 1 doi:10.1088/2041-8205/718/2/L117

THE CONSTANT INNER-DISK RADIUS OF LMC X-3: A BASIS FOR MEASURING BLACK HOLE SPIN

James F. Steiner[1], Jeffrey E. McClintock[1], Ronald A. Remillard[2], Lijun Gou[1], Shin'ya Yamada[3], and Ramesh Narayan[1]
[1] Harvard-Smithsonian Center for Astrophysics, 60 Garden Street, Cambridge, MA 02138, USA; jsteiner@cfa.harvard.edu
[2] MIT Kavli Institute for Astrophysics and Space Research, MIT, 70 Vassar Street, Cambridge, MA 02139, USA
[3] Department of Physics, University of Tokyo, 7-3-1 Hongo, Bunkyo-ku, Tokyo 113-0033, Japan
Received 2010 January 25; accepted 2010 June 28; published 2010 July 9

ABSTRACT

The black hole binary system LMC X-3 has been observed by virtually every X-ray mission since the inception of X-ray astronomy. Among the persistent sources, LMC X-3 is uniquely both habitually soft and highly variable. Using a fully relativistic accretion disk model, we analyze hundreds of spectra collected during eight X-ray missions that span 26 years. For a selected sample of 391 *RXTE* spectra, we find that to within ≈2% the inner radius of the accretion disk is constant over time and unaffected by source variability. Even considering an ensemble of eight X-ray missions, we find consistent values of the radius to within ≈4%–6%. Our results provide strong evidence for the existence of a fixed inner-disk radius. The only reasonable inference is that this radius is closely associated with the general relativistic innermost stable circular orbit. Our findings establish a firm foundation for the measurement of black hole spin.

Key words: accretion, accretion disks – black hole physics – stars: individual (LMC X-3) – X-rays: binaries

1. INTRODUCTION

The X-ray binary LMC X-3 was discovered by *Uhuru* in 1971 (Leong et al. 1971). Observations of its B3V optical counterpart revealed an orbital period of 1.7 days and a mass function of $2.3 \pm 0.3\,M_{\odot}$. Because of its massive companion star, this established LMC X-3 as a strong dynamical black hole (BH) candidate (Cowley et al. 1983; Kuiper et al. 1988). Subsequent X-ray observations spanning decades have revealed a complex behavioral pattern that includes transitions between soft and hard states (Wilms et al. 2001) and long-term ($\gtrsim$100 days) variability cycles (Cowley et al. 1991). While by some metrics LMC X-3 is a nearly archetypal BH binary, its combined qualities of persistence and strong variability set it apart as unique.

Among the BH systems, LMC X-3 bridges the divide between low-mass X-ray binaries powered by Roche lobe overflow and wind-fed, high-mass X-ray binaries (Soria et al. 2001). The former are transients, usually locked in a deep quiescent state, whereas the latter systems are persistently X-ray bright. Among the classical persistent BH sources (Cyg X-1, LMC X-1, and LMC X-3), LMC X-3 habitually shows the softest X-ray spectrum, reaches the highest luminosity, and exhibits the largest variations in intensity.

Because of its persistence, LMC X-3 has been observed by nearly every X-ray astronomy mission. In this Letter, we apply our relativistic accretion disk model (kerrbb2; McClintock et al. 2006) to essentially all available X-ray data in order to examine the presumed constancy of the inner radius of the BH's accretion disk. We draw upon data collected by eight missions, with *RXTE* providing the lion's share.

For thin accretion disks, recent magnetohydrodynamic simulations provide support for identifying the inner-disk radius $R_{\rm in}$ with the radius of the innermost stable circular orbit $R_{\rm ISCO}$ (Reynolds & Fabian 2008; Shafee et al. 2008; Penna et al. 2010; but see Noble et al. 2009), a proposition that has a long history of theoretical and observational support (e.g., see Section 6 in Gou et al. 2009). With this identification and the simple monotonic relationship between $R_{\rm ISCO}$ and the BH spin parameter (Shapiro & Teukolsky 1983), a measurement of $R_{\rm in}$ is equivalent to a measurement of the spin of the BH. This is the basis for both the continuum-fitting (Zhang et al. 1997) and Fe–K (Fabian et al. 1989) methods of measuring spin. In recent years, both methods have been used to estimate the spins of stellar BHs (e.g., Shafee et al. 2006; McClintock et al. 2006; Davis et al. 2006; Reis et al. 2008; Miller et al. 2009; Blum et al. 2009).

The mass of LMC X-3's BH primary is presently very uncertain (Cowley 1992), and we adopt a round value that is typical for BH binaries of $M = 10\,M_{\odot}$. For the inclination, we adopt the provisional value $i = 67^{\circ}$ (Kuiper et al. 1988). Because of the uncertainties in both M and i, in this Letter we do not attempt to estimate the BH's spin. Rather, we assume a reasonable value for the mass and employ the X-ray continuum-fitting method in order to study the constancy of $R_{\rm in}$. We describe our data set comprised of hundreds of multi-mission spectra in Section 2 and our analysis in Section 3, and present our results in Section 4. In Section 5, we explore the systematics associated with our spectral model and conclude by discussing our results in the context of ongoing studies of BH spin.

2. OBSERVATIONS

RXTE. The *Rossi X-ray Timing Explorer* (*RXTE*) is our workhorse instrument, providing a total gross sample of 712 spectra. Individual spectra were defined by grouping all the archival pointed data from 1996 to 2009 into approximately half-day bins with ≈90% of exposure times ranging from 1 to 10 ks. We only use pulse-height spectra obtained by the best-calibrated Proportional Counter Array (PCA) detector, PCU-2 (Jahoda et al. 2006). Count rates have been renormalized to correct for detector dead time, and a systematic error of 1% has been included to account for uncertainty in the instrumental response (Jahoda et al. 2006). These data have been analyzed from 2.55 to 25 keV over all reliable gain epochs (≥epoch 2).

Here and elsewhere, the analysis work has been performed using XSPEC v.12.5.1o (recent enough that an early coding error in kerrbb has been fixed[4]; Arnaud 1996).

EXOSAT. Seven observations from 1983 to 1984 were obtained via the HEASARC archive[5]; only data from the Medium Energy Instrument (ME) are currently available. Spectra were extracted as described in Treves et al. (1988) and analyzed from 1 to 25 keV. The customary systematic error of 1% was included.

Ginga. The Large Area Counter (LAC) observed LMC X-3 on 18 occasions during 1987–1990. To extract these spectra, we followed the procedures described in Ebisawa et al. (1993). Each spectrum has been analyzed from 1.5 to 25 keV with a 1% systematic error included.

ASCA. LMC X-3 was observed twice, once on UT 1993 September 22 and later on UT 1995 April 14. We extracted and separately combined spectra from the two Gas Imaging Spectrometer (GIS) and two Solid-state Imaging Spectrometer (SIS) instruments. Data were calibrated relative to the GIS-2 detector and analyzed from 0.8 to 9 keV(GIS) and 0.6 to 9 keV(SIS) using a 2% systematic uncertainty.

BeppoSAX. Following the standard reduction guide (Fiore et al. 1999), we have generated spectra for the narrow-field instruments from each of the 23 available observations. We extracted spectra using 8′ apertures in the imaging instruments and used a fixed rise-time threshold for the Phoswich Detector System (PDS). For each observation, we employed all usable Law Energy Concentrator Spectrometer (LECS), Medium Energy Concentrator Spectrometer (MECS), and PDS data. Throughout, we adopted the standard inter-detector floating normalizations calibrated relative to the MECS. Data were analyzed from 0.12 to 4 keV (LECS), 1.65 to 10 keV (MECS), and 15 to 80 keV (PDS). A 1% systematic error has been included.

XMM-Newton. All photon-counting data were severely piled up and therefore rejected because of uncertainties in the flux calibration. We use the single available 19 ks timing-mode observation of LMC X-3 obtained on UTC 2000 November 25. Because of the large number of accumulated counts, $\sim 2 \times 10^6$, uncertainties in the response of the detector are dominant, and we therefore included a 3% systematic error and fitted over 0.5–10 keV. Reduction and processing has been performed using *XMM* SAS v9.0.0.[6]

Swift. The sole X-ray Telescope (XRT) windowed-timing mode observation of LMC X-3, taken on UTC 2007 November 26, has been procured and analyzed following the procedures outlined in Capalbi et al. (2005). We rejected all the photon-counting data because they suffer from extreme pileup. Calibration version 11 files have been used for the data reduction. In consultation with the *Swift* Help Desk, we have included an extra model component to account for an instrumental artifact near the Si edge around 1.7 keV. Analysis has been conducted over 0.4–10 keV using a 1% systematic error.

Suzaku. Two observations were made on 2008 December 22 and 2009 December 21 (UT). The *Suzaku* attitude calibration was improved using the *AEattcor* routine.[7] We applied the appropriate reduction procedures for a bright point source.[8] Pileup was kept well below ∼3% by excluding the innermost 10″ and 30″ for the 2008 and 2009 observations, respectively. In all other respects, we have followed the methods of Kubota et al. (2010), including using their energy intervals and adopting a 1% systematic error. A fixed cross-normalization of 1.16 is used between X-ray Imaging Spectrometer and Hard X-ray Detector-PIN detectors (Maeda et al. 2008).

Table 1
Data and Instrument Summary

Instrument	N_{obs}	N_{sel}[a]	f_{TS}[b]	$\Delta\Gamma_{TS}$[b]	Ref.
RXTE (PCU-2)	712	391 (568)	1.097	0.010	...
Suzaku (XIS0)	2	2 (2)	0.98	−0.01	1,2
Swift (XRT)	1	1 (1)	1.01	−0.04	3[c]
XMM (MOS-1)	1	0 (1)	1.00	0.01	4,5,6
BeppoSAX (MECS)	23	2 (23)	0.95	0.00	7
ASCA (GIS-2)	2	2 (2)	0.97	−0.01	8,9
Ginga (LAC)	18	7 (11)	0.94	−0.02	10
EXOSAT (ME)	7	6 (6)	0.98	0.00	11

Notes.
[a] Number of selected observations. Parentheses indicate the selection numbers when high luminosities $l_D > 0.3$ are allowed (see Figure 2).
[b] f_{TS} is the ratio of the Crab normalization to that of Toor & Seward and $\Delta\Gamma_{TS}$ is the difference between photon indices.
[c] The *Swift* values are derived from a comparison between *RXTE* and *Swift* observations of 3C 273.
References. (1) Serlemitsos et al. 2007; (2) http://heasarc.gsfc.nasa.gov/docs/suzaku/prop_tools/suzaku_td.html; (3) Godet et al. 2009; (4) Guainazzi et al. 2009; (5) Stuhlinger et al. 2006; (6) I. de la Calle 2009, private communication; (7) Fiore et al. 1999; (8) Makishima et al. 1996; (9) Ebisawa 1996; (10) Turner et al. 1989; (11) Parmar & Smith 1985.

2.1. Flux Calibration

Just as deducing the radius of a star from its spectrum requires knowledge of its luminosity, in order to estimate the inner radius of an accretion disk it is also necessary to determine its luminosity. However, the measurement of X-ray luminosity is problematic in X-ray astronomy because of the significant flux-normalization differences, often $\gtrsim$10%, between missions. We address this issue by using the power-law spectrum of the Crab Nebula as measured by Toor & Seward (1974): $\Gamma = 2.1$ and $N = 9.7$ photons s^{-1} keV^{-1} at 1 keV.

For each mission considered herein (excepting *Swift*; see Table 1), we either rely on the Crab calibration performed by the instrument team or we compute a correction to the effective area by comparing the spectrum predicted by Toor & Seward (1974) to parameters obtained by analyzing proximate, archival observations of the Crab. Toor & Seward normalization coefficients f_{TS} and slope differences $\Delta\Gamma_{TS}$ are presented for each mission in Table 1. This table also summarizes for LMC X-3 the gross number of observations available from each mission, N_{obs}, as well as the number of observations that meet our selection criteria, N_{sel} (Section 3.1).

3. ANALYSIS

At energies above ∼5–10 keV, the spectra of BH binaries in all states show a contribution from a power-law component. This power law is widely attributed to inverse Compton scattering of thermal disk photons by hot coronal electrons. The power-law model we employ, SIMPL, generates this Compton component by upscattering seed photons from the thermal component (Steiner et al. 2009b).

[4] http://heasarc.nasa.gov/docs/xanadu/xspec/issues/archive/issues.12.5.0an.html
[5] http://heasarc.nasa.gov
[6] http://xmm.esac.esa.int/sas/
[7] http://space.mit.edu/CXC/software/suzaku/
[8] http://www.astro.isas.ac.jp/suzaku/analysis/xis/pileup/HowToCheckPileup_v1.pdf

The thermal and principal component of our model is KERRBB2, a thin accretion disk model that includes all relativistic effects, self-irradiation of the disk ("returning radiation"), limb darkening, and the effects of spectral hardening (Li et al. 2005; McClintock et al. 2006). During analysis, this latter effect is handled on the fly via a look-up table of the spectral hardening factor f for a given value of the disk viscosity parameter α (we adopt $\alpha = 0.01$ as default). These tables were computed using BHSPEC, a second relativistic disk model (Davis et al. 2006; Davis & Hubeny 2006).

Our fit to the thermal component of the spectrum effectively determines the solid angle subtended by the accretion disk: $\Omega = \pi(R_{\rm in}/D)^2 \cos i$, where D is the distance and i is the inclination of the accretion disk with respect to the line of sight. For D, we use the average distance to the LMC, $D = 48.1$ kpc (e.g., Orosz et al. 2009), while for inclination we use $i = 67^\circ$ (Section 1). Finally, we express $R_{\rm in}$ in dimensionless form, $r_{\rm in} \equiv R_{\rm in}/(GM/c^2)$ using $M = 10\,M_\odot$ (Section 1). We have recently shown that the choice of M, i, and D, which effectively sets the absolute scale for $r_{\rm in}$ and the luminosity, is quite unimportant for testing the stability of $r_{\rm in}$ (see Figure 3 and text in Steiner et al. 2009a). (These values are crucial, however, when it comes to estimating the spin of the BH.)

Using our adopted values of the source M, i, and D, our source model has four fit parameters: two for KERRBB2, $R_{\rm in}$ and the mass accretion rate $\dot{M}$, and two for SIMPL, the photon index Γ and $f_{\rm SC}$, which is the fraction of disk photons that get re-directed via scattering into the power law. Our full model is TBABS(SIMPL⊗KERRBB2), where TBABS models the effects of photoelectric absorption; we fix its sole parameter: $N_{\rm H} = 4 \times 10^{20}$ cm^{-2} (Page et al. 2003), using abundances from Wilms et al. (2000). For KERRBB2 we include limb darkening and returning radiation effects, set the torque at the inner boundary of the accretion disk to zero, and fix the normalization to unity. We use the efficient, upscattering-only version of SIMPL, and in Section 5 we show that this choice is unimportant.

3.1. Data Selection

Our preliminary analysis of all the data showed that for many spectra the power-law index Γ was essentially unconstrained, even for the *BeppoSAX*, *EXOSAT*, *Ginga*, and *RXTE* missions, which have the requisite coverage to detect this component. This is because the source is relatively faint ($\lesssim$ 50 mCrab) and its Compton power-law component is generally very weak, showing a median normalization $f_{\rm SC} \approx 0.3\%$. The extreme dominance of the thermal component in LMC X-3 makes it an ideal source for accretion disk studies like this.

Restricting our census to the 134 *RXTE* spectra for which the photon index is measured to a precision better than $\sigma_\Gamma = 0.5$, we find a strong clustering of values in the range $\Gamma \approx$ 2–2.6. For our baseline model, we fix $\Gamma = 2.35$ which matches the constant index derived from 22 deep *RXTE* pointings by Smith et al. (2007), and in Section 5, we show that our results depend very weakly on this choice for $2 \lesssim \Gamma \lesssim 3$.

Meanwhile, three missions, *ASCA*, *Swift*, and *XMM*, have no sensitivity above $E \approx 10$ keV, and therefore only very loosely measure the power-law normalization parameter, $f_{\rm SC}$. At the same time, a self-consistent and fruitful analysis of the thermal and Compton components requires that $f_{\rm SC}$ be sensibly constrained. Therefore, and because the power law is generally so weak, we impose an additional data-selection requirement, namely, that for each fit $f_{\rm SC}$ falls within the lower 95% span of the *RXTE* rank-ordered values.

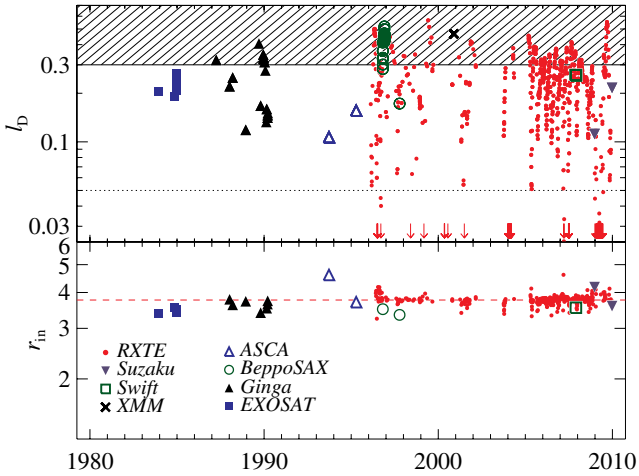

Figure 1. Top: accretion disk luminosity in Eddington-scaled units ($M = 10\,M_\odot$) vs. time for all the data considered in this study (766 spectra). Red arrows show *RXTE* data which are off scale. Data in the unshaded region satisfy our thin-disk selection criterion ($H/R < 0.1$, which implies $l_{\rm D} < 0.3$; McClintock et al. 2006). The dotted line indicates the lower luminosity threshold (5% $L_{\rm Edd}$) adopted in Section 3.1. Bottom: values of the dimensionless inner-disk radius $r_{\rm in}$ are shown for thin-disk data in the top panel that meet all of our selection criteria (411 spectra; see Section 3.1). Despite large variations in luminosity, $r_{\rm in}$ remains constant to within ≈4% over time. The median value for the *RXTE* data alone ($r_{\rm in} = 3.77$) is shown as a red dashed line.

We further adopt a goodness-of-fit requirement, $\chi^2/\nu < 2$, and a lower limit on the Eddington-scaled disk luminosity, $l_{\rm D} \equiv L_{\rm D}/L_{\rm Edd} > 0.05$. This latter criterion removes any hard-state data in which the disk is likely truncated at $r > r_{\rm in}$ (e.g., Esin et al. 1997). Finally, in consonance with the thin-disk model employed, we only select data for which $l_{\rm D} < 0.3$ (McClintock et al. 2006).

4. RESULTS

The top panel of Figure 1 shows a 26 year record of the disk luminosity of LMC X-3, which is seen to vary by orders of magnitude. Two-thirds of the data meet our thin-disk selection criterion $l_{\rm D} < 0.3$. In the lower panel, we show the time history of the inner-disk radius $r_{\rm in}$ for just those data that meet all of our selection criteria (Section 3.1). The radius is constant over the 26 years of monitoring to within ∼2% for *RXTE* alone and ∼4% considering all missions.

Figure 2 explores the dependence of $r_{\rm in}$ on luminosity. In this figure, we include the high-luminosity data ($l_{\rm D} > 0.3$) that meet all of our other selection criteria (Section 3.1). For $l_{\rm D} < 0.3$ there is a gentle, nonlinear rise of $r_{\rm in}$ with luminosity. Especially visible in the *RXTE* data, this rise becomes prominent beyond $l_{\rm D} \sim 0.25$, above which there is a ∼12% increase in $r_{\rm in}$. No significant change in χ^2/ν is associated with the apparent increase of $r_{\rm in}$. We cannot say if this represents a real increase in $r_{\rm in}$ at high luminosities or is simply an artifact of using the thin-disk model, which is expected to be increasingly inaccurate at higher luminosities (Penna et al. 2010; Abramowicz et al. 2010) at which a transition may occur to an advective slim-disk accretion mode. Interestingly, however, despite this rapid rise, we note that the *RXTE* data appear tightly clustered along a well-defined curve. We approximate this dependence using a non-parametric curve fit (LOWESS; Cleveland 1979) that allows us to detrend the data. We conclude that results from all eight missions, including the high-luminosity data, are in agreement with one another to within ≈6%.

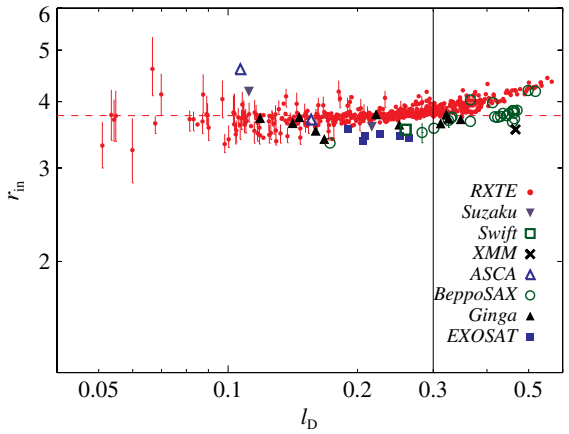

Figure 2. Dimensionless inner-disk radius r_{in} vs. luminosity for the filtered data (Section 3.1) and our baseline model. The vertical black line shows our adopted thin-disk upper limit, $l_D = 0.3$. As in Figure 1, the red dashed line shows the *RXTE* average below this limit.

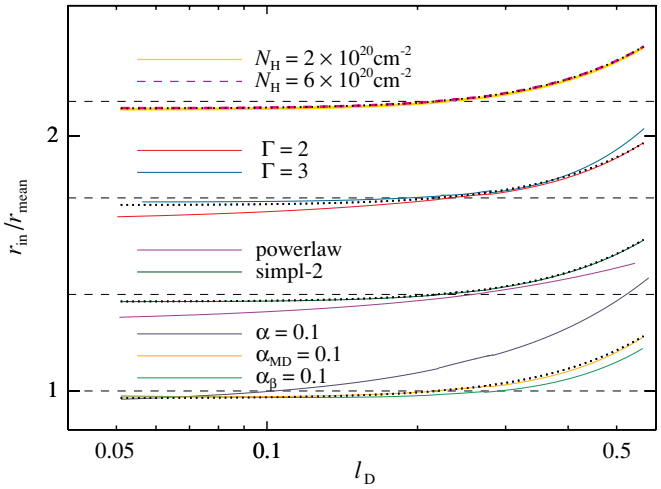

Figure 3. Four families of models showing how our baseline results in Figure 2 are affected when a single model component or parameter is varied. The black dotted line drawn with each family of curves represents our fiducial model: $N_H = 4 \times 10^{20}$ cm^{-2}; $\Gamma = 2.35$; SIMPL-1; and $\alpha = 0.01$. The horizontal dashed line for each family is set by the average value of r_{in} (see Figures 1 and 2), and each family is offset by 30% for clarity. Each curve represents a LOWESS curve fit to the *RXTE* data alone. Both axes are scaled logarithmically.

5. DISCUSSION

Figure 2 clearly demonstrates the limitations of the thin-disk model at high luminosities. We further illustrate this point in Figure 3 using LOWESS fits to the abundant *RXTE* data. We vary, one-at-a-time, the model components and parameters of our baseline model, grouping these trials into four separate "families." In order of increasing importance, these families are (1) column density N_H, (2) power-law index Γ, (3) choice of power-law model, and (4) α. Figure 3 illustrates the changes introduced by adjusting each family of settings.

We highlight two conclusions from Figure 3: (1) our results are relatively insensitive to all settings with the single exception of the choice of α-viscosity; the value $\alpha = 0.1$ increases significantly the dependence of r_{in} on luminosity. (2) The positive correlation between r_{in} and luminosity is generally present for all families over the full range of luminosity, but it becomes prominent only above $l_D \approx 0.2$–0.3.

Inspecting the families of curves in Figure 3 from top to bottom, one concludes the following: as the first two families show, our results are insensitive to the choice of N_H and only modestly sensitive to the choice of Γ. In modeling the Compton tail component (third family), one sees that our results are essentially identical whether one uses our baseline upscattering-only model SIMPL ≡SIMPL-1 or a two-sided scattering model SIMPL-2 (Steiner et al. 2009a), while the results obtained using the standard power-law model POWERLAW differ only modestly ($\lesssim$5%).

The fourth family considers the primary setting for BHSPEC, the viscosity parameter α, used to compute spectral hardening (Section 3). Here, we examine several distinct cases: our fiducial value, $\alpha = 0.01$ (dotted), the value $\alpha = 0.1$ (Section 3; dark blue), and alternative stress prescriptions $\alpha_{MD} = 0.1$ (orange) and $\alpha_\beta = 0.1$ (green). The parameter α typically refers to viscosity in the disk which is proportional to the total pressure at the disk mid-plane. However, other choices exist such as "beta disk" and "mean disk" models in which α_β and α_{MD}, respectively, describe viscosities which scale proportionally to the gas pressure or the geometric mean of the gas and total pressures (Done & Davis 2008). Both latter options produce spectral hardening values quite similar to those obtained for $\alpha = 0.01$. In conclusion, only the second option, $\alpha = 0.1$, has an important effect on our results.

Our results indicate that the value of the inner-disk radius r_{in}—and hence spin—is stable over decades, as is expected given the minute effects of accretion torques on a BH over such a timescale. We also confirm that r_{in} is nearly independent of luminosity provided that the disk is geometrically thin. The stability of r_{in} over time (for $l_D < 0.3$) despite large fluctuations in the mass accretion rate provides strong evidence that r_{in} and R_{ISCO} are closely associated, as we tacitly assume in measuring BH spin (Section 1).

The inter-mission consistency of our results (≈4% below $l_D < 0.3$ and 6% overall) is very important for future X-ray continuum measurements of BH spin: for some transient BH sources (e.g., A0620–00 and GRS 1009–45), only one or a few spectra are available in the data archives. Our results for LMC X-3 show that, as long as the power-law component is reliably measured, even a single, suitable spectrum can deliver an estimate of the disk inner radius accurate to several percent, and thereby a reliable measurement of spin.

This research has made use of data obtained from the High Energy Astrophysics Science Archive Research Center (HEASARC), provided by NASA's Goddard Space Flight Center. We thank Shane Davis and Laura Brenneman for their insightful analyses of the manuscript and suggestions. J.F.S. thanks Tim Oosterbroek for assisting with *BeppoSAX* LECS, and Ignacio de la Calle for advice on *XMM*. The authors thank Tomaso Belloni and Ken Ebisawa for contributing reduced archival data from *EXOSAT*, and *Ginga* and *ASCA*, respectively. J.F.S. was supported by the Smithsonian Institution Endowment Funds, and J.E.M. acknowledges support from NASA grant NNX08AJ55G. R.N. acknowledges support from NASA grant NNX08AH32G and NSF grant AST-0805832.

REFERENCES

Abramowicz, M. A., Jaroszynski, M., Kato, S., Lasota, J., Rozanska, A., & Sadowski, A. 2010, arXiv:1003.3887

Arnaud, K. A. 1996, in ASP Conf. Ser. 101, Astronomical Data Analysis Software and Systems V, ed. G. H. Jacoby & J. Barnes (San Francisco, CA: ASP), 17

Blum, J. L., Miller, J. M., Fabian, A. C., Miller, M. C., Homan, J., van der Klis, M., Cackett, E. M., & Reis, R. C. 2009, ApJ, 706, 60
Capalbi, M., Perri, M., Saija, B., Tamburelli, F., & Angelini, L. 2005, The Swift XRT Data Reduction Guide, Technical Report 1.2
Cleveland, W. S. 1979, J. Am. Stat. Assoc., 74, 829
Cowley, A. P. 1992, ARA&A, 30, 287
Cowley, A. P., Crampton, D., Hutchings, J. B., Remillard, R., & Penfold, J. E. 1983, ApJ, 272, 118
Cowley, A. P., et al. 1991, ApJ, 381, 526
Davis, S. W., Done, C., & Blaes, O. M. 2006, ApJ, 647, 525
Davis, S. W., & Hubeny, I. 2006, ApJS, 164, 530
Done, C., & Davis, S. W. 2008, ApJ, 683, 389
Ebisawa, K. 1996, Release of New XRT Responses, and Comparison of ascaarf v2.53 and v2.62, Technical Report
Ebisawa, K., Makino, F., Mitsuda, K., Belloni, T., Cowley, A. P., Schmidtke, P. C., & Treves, A. 1993, ApJ, 403, 684
Esin, A. A., McClintock, J. E., & Narayan, R. 1997, ApJ, 489, 865
Fabian, A. C., Rees, M. J., Stella, L., & White, N. E. 1989, MNRAS, 238, 729
Fiore, F., Guainazzi, M., & Grandi, P. 1999, Cookbook for BeppoSAX NFI Spectral Analysis, Bepposax SDC (Greenbelt, MD: NASA GSFC), http://heasarc.gsfc.nasa.gov/docs/sax/abc/saxabc/saxabc.html
Godet, O., et al. 2009, A&A, 494, 775
Gou, L. J., et al. 2009, ApJ, 701, 1076
Guainazzi, M., Kirsch, M., & Haberl, F. 2009, Evaluation of the Spectral Calibration Accuracy in EPIC-pn Fast Modes, Technical Report CAL-TN-0083, XMM-Newton Science Operations Center
Jahoda, K., Markwardt, C. B., Radeva, Y., Rots, A. H., Stark, M. J., Swank, J. H., Strohmayer, T. E., & Zhang, W. 2006, ApJS, 163, 401
Kubota, A., Done, C., Davis, S. W., Dotani, T., Mizuno, T., & Ueda, Y. 2010, ApJ, 714, 860
Kuiper, L., van Paradijs, J., & van der Klis, M. 1988, A&A, 203, 79
Leong, C., Kellogg, E., Gursky, H., Tananbaum, H., & Giacconi, R. 1971, ApJ, 170, L67
Li, L.-X., Zimmerman, E. R., Narayan, R., & McClintock, J. E. 2005, ApJS, 157, 335
Maeda, Y., et al. 2008, Recent Update of the XRT Response. III. Effective Area, Technical Report Suzaku Memo 2008-06, JX-ISAS
Makishima, K., et al. 1996, PASJ, 48, 171
McClintock, J. E., Shafee, R., Narayan, R., Remillard, R. A., Davis, S. W., & Li, L.-X. 2006, ApJ, 652, 518
Miller, J. M., Reynolds, C. S., Fabian, A. C., Miniutti, G., & Gallo, L. C. 2009, ApJ, 697, 900
Noble, S. C., Krolik, J. H., & Hawley, J. F. 2009, ApJ, 692, 411
Orosz, J. A., et al. 2009, ApJ, 697, 573
Page, M. J., Soria, R., Wu, K., Mason, K. O., Cordova, F. A., & Priedhorsky, W. C. 2003, MNRAS, 345, 639
Parmar, A., & Smith, A. 1985, ME Calibration and Updates to the CCF, Technical Report, EXOSAT Express
Penna, R. F., McKinney, J. C., Narayan, R., Tchekhovskoy, A., Shafee, R., & McClintock, J. E. 2010, MNRAS, in press (arXiv:1003.0966)
Reis, R. C., Fabian, A. C., Ross, R. R., Miniutti, G., Miller, J. M., & Reynolds, C. 2008, MNRAS, 387, 1489
Reynolds, C. S., & Fabian, A. C. 2008, ApJ, 675, 1048
Serlemitsos, P. J., et al. 2007, PASJ, 59, 9
Shafee, R., McClintock, J. E., Narayan, R., Davis, S. W., Li, L.-X., & Remillard, R. A. 2006, ApJ, 636, L113
Shafee, R., McKinney, J. C., Narayan, R., Tchekhovskoy, A., Gammie, C. F., & McClintock, J. E. 2008, ApJ, 687, L25
Shapiro, S. L., & Teukolsky, S. A. 1983, Black Holes, White Dwarfs, and Neutron Stars: The Physics of Compact Objects (New York: Wiley-Interscience)
Smith, D. M., Dawson, D. M., & Swank, J. H. 2007, ApJ, 669, 1138
Soria, R., Wu, K., Page, M. J., & Sakelliou, I. 2001, A&A, 365, L273
Steiner, J. F., McClintock, J. E., Remillard, R. A., Narayan, R., & Gou, L. J. 2009a, ApJ, 701, L83
Steiner, J. F., Narayan, R., McClintock, J. E., & Ebisawa, K. 2009b, PASP, 121, 1279
Stuhlinger, M., et al. 2006, Status of XMM-Newton Instruments Cross-Calibration with SASv6.5, Technical Report CAL-TN-0052v3, XMM-Newton Science Operations Center
Toor, A., & Seward, F. D. 1974, AJ, 79, 995
Treves, A., Belloni, T., Chiappetti, L., Maraschi, L., Stella, L., Tanzi, E. G., & van der Klis, M. 1988, ApJ, 325, 119
Turner, M. J. L., et al. 1989, PASJ, 41, 345
Wilms, J., Allen, A., & McCray, R. 2000, ApJ, 542, 914
Wilms, J., Nowak, M. A., Pottschmidt, K., Heindl, W. A., Dove, J. B., & Begelman, M. C. 2001, MNRAS, 320, 327
Zhang, S. N., Cui, W., & Chen, W. 1997, ApJ, 482, L155